Materials and Design 200 (2021) 109443

Contents lists available at ScienceDirect

Materials and Design

journal homepage: www.elsevier.com/locate/matdes

Graphene oxide (GO) decorated on multi-structured porous titania fabricated by plasma electrolytic oxidation (PEO) for enhanced antibacterial performance

Arash Mazinani [a,b], Md Julker Nine [a,b], Roberto Chiesa [c], Gabriele Candiani [c], Paolo Tarsini [c], Tran Thanh Tung [a,b], Dusan Losic [a,b,*]

[a] School of Chemical Engineering and Advanced Materials, The University of Adelaide, Adelaide, SA 5005, Australia
[b] ARC Hub for Graphene Enabled Industry Transformation, The University of Adelaide, Adelaide, SA 5005, Australia
[c] Department of Chemistry, Materials and Chemical Engineering "G. Natta", Politecnico di Milano, Via Mancinelli 7, Milano 20131, Italy

HIGHLIGHTS

- Plasma Electrolytic Oxidation (PEO) and Electrophoretic Deposition (ED) are combined for Graphene Oxide deposition (GO).
- Partial deposition of (GO) sheets on PEO anodized titanium as new antibacterial surface is demonstrated.
- The optimized deposition with 60% GO surface coverage is found as the best performing.
- Antibacterial activity ~80% against *E.coli* and ~100% against *S. aureus* bacteria is achieved.

GRAPHICAL ABSTRACT

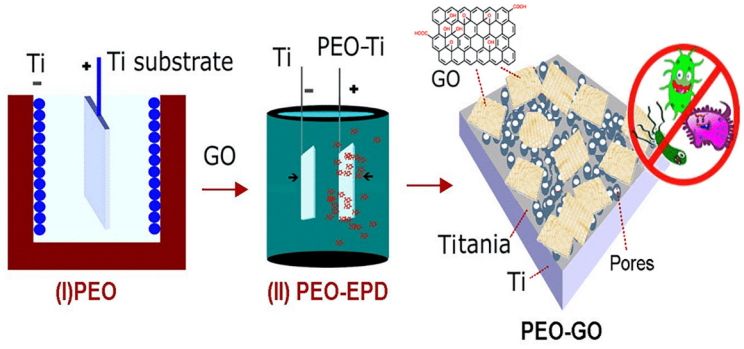

ARTICLE INFO

Article history:
Received 4 July 2020
Received in revised form 23 December 2020
Accepted 28 December 2020
Available online 31 December 2020

Keywords:
Antibacterial surfaces
Plasma electrolytic oxidation
Electrophoretic deposition
Graphene oxide

ABSTRACT

Plasma electrolytic oxidation (PEO) is proven as a scalable method for surface treatment of titanium (Ti) providing a thick oxide layer with porous micro-nano morphology. Despite the lack of antibacterial performance, this modification has potential to improve the osseointegration properties of Ti-based implant. To address this limitation, we demonstrated a new concept, showing that partial incorporation of graphene oxide (GO) to porous-PEO Ti-surface can significantly improve its antibacterial performance. Our idea for partial coating compared with a full surface coverage of GO was motivated to create a mixed surface with porous PEO and GO to improve antibacterial ability, while maintaining the osseointegration properties. To achieve these goals, we combined PEO and electrophoretic deposition process (EPD) to deposit GO sheets over the titanium PEO-treated substrate. The SEM, EDS, optical profilometry, XRD and Raman spectroscopy confirmed the growth of unique multi-structured porous PEO structures decorated with GO patches. The bio-mineralization test provided the evidence of hydroxyapatite formation over the PEO-GO surface, indicating its good bioactivity. Finally, PEO-GO samples demonstrated a superior antibacterial rate of ~80% against *E.coli* and ~100% against *S. aureus*. These results indicate that PEO-GO modified titanium substrates are very promising for the development of advanced biomedical implants.

1. Introduction

Over the years, titanium (Ti) and Ti-alloys have replaced many other common metals such as magnesium (Mg) alloy and stainless steel used

* Corresponding author at: School of Chemical Engineering and Advanced Materials, The University of Adelaide, Adelaide, SA 5005, Australia.
E-mail address: dusan.losic@adelaide.edu.au (D. Losic).

https://doi.org/10.1016/j.matdes.2020.109443

in the bio-implants production. Nowadays, Ti is considered as the first choice for a number of biomedical applications such as dental implants, bone implants and localized drug delivery systems due to its excellent durability, corrosion resistance, mechanical strength, low specific weight and biocompatibility [1–3]. Despite being a "valve metal" with suitable biocompatible property, the rejection of Ti-based implants as a result of poor bio-integration and bacterial infection are concerning. Additionally, it is causing significant healthcare costs and devastating impact on patients [4–6]. The osseointegration property of Ti-implant has a crucial role in bone bonding and improving the implant lifetime, which is mainly influenced by Ti-implant composition and the applied surface treatment [7,8]. To improve osseointegration properties, the surface of commercial implants is usually modified by different methods such as hydroxyapatite coating (HAp), micro-roughening by chemical etching, grit-blasting, laser micro-machining and powder coating [9–12]. Moreover, many other micro and nano fabrication methods (including electrochemical anodization, Plasma Electrolytic Oxidation (PEO) also known as Micro Arc Oxidation (MAO), hydrothermal process, polymer coatings, etc.) were explored to improve the bioactivity of implants [13–16]. Among them, PEO surface modification of Ti-alloy is demonstrated to be a very successful scalable process, which was introduced in dental and orthopaedic fields, showing excellent outcome in the osseointegration improvement [8,17]. The PEO roughened surface with a unique combination of micro-nano pores provides suitable sites for ingrowth of bone tissue, which can accelerate bone-implant bonding and improves mechanical anchoring of implants [7]. This unique method is working based on the generation of micro arcs, resulted from the application of high electric field in an electrolytic solution, that bombards the valve metals surface locally and forms a protective oxide layer dominated with micro-nano structure morphology [18–21]. However, apart from the improved osseointegration properties of PEO treated Ti-implant, the problem with low antibacterial protection remains unsolved [22].

Graphene derivatives (e.g. graphene, graphene oxide (GO), reduced graphene oxide (rGO), doped and other functionalized graphene) with a variety of extraordinary mechanical, and physiochemical properties opened their way into the versatile applications such as multifunctional-coating [23], photocatalysts [24], composites [25,26], supercapacitors [27] and environmental application [28]. Among many graphene derivatives, GO and rGO have recently drawn a significant attention in the biomedical and antimicrobial fields after revealing their potential to be efficient antimicrobial nanomaterials [29,30]. Antibacterial studies using different types of graphene-based materials against *Escherichia coli (E.coli)* showed that GO has the highest antimicrobial properties, followed by rGO, graphite, and graphite oxide [31]. Research has been carried out to understand the mechanisms behind the antibacterial activity of graphene-based materials towards gram-negative and gram-positive bacteria. The proposed mechanisms are still the subject of great interest for researchers, which are principally based on the formation of reactive oxygen species (ROS), and oxidative stress along with possessing sharp edges identified to be effective in the antimicrobial activity of GO and rGO. Additional parameters such as hydrophobicity and surface roughness along with the mode of contact between the basal plane of graphene derivatives and bacteria were found to be effective on the antimicrobial properties of these materials [32,33]. Meanwhile, It has been shown that GO has a potential to promote mechanical stability of coatings by decreasing the number of microcracks and also has an ability to enhance the bioactivity via improving the adhesion and proliferation of bone cell unites so-called osteoblasts [34–36]. Based on these promising results, efforts have been made to form and implement graphene-based composite to tackle microbial Multidrug Resistance (MDR), such as *Klebsiella pneumonia*, and to improve the antibacterial activity of Ti-implants [33,37]. In order to deposit graphene derivatives on the metallic implants, different methods such as dip-coating, plasma coating, spray-coating, electrophoretic deposition (EPD), anodization-EPD, anodization-hydrothermal, etc. have been explored [38–41].

Recently, several studies were carried out to incorporate GO to the PEO matrix of light metals such as Al and Ti [42–44], to improve their interfacial performance and functionality. However, the presence of GO over the coating is not evident, while only a few random deposition sites are differentiable over the substrate [42,44]. Other studies suggest that the generation of micro-nano bubbles during the PEO process at electrodes may impede the attachment of GO flakes to the substrate [45,46]. Other researchers also investigated new approaches to immobilize GO sheets over the PEO surface, such as application of APTE to fabricate GO thin film on the surface. Their results demonstrated the great potential of GO continuous film on the PEO surface for killing gram-positive bacteria such as *S. mutans* [22].

The EPD is a fast and straightforward process that allows deposition of GO over the metallic surface [45,46]. To date, several studies conducted to deposit GO-based continuous films over biomaterials such as Ti and Mg utilizing EPD technique [47,48]. Unfortunately, the low voltage EPD technique suffers weakened adhesion between the coating and the substrate [49]. Notably, the presence of a thick oxide layer on PEO substrate limits the deposition yield of GO with common EPD techniques. As a potential solution for this problem, Nie et al. [50] suggested a hybrid technique by the combination of PEO and EPD known as PEO-EPD process. This combined method has shown a great potential to tackle poor adhesion problem of bioceramics on valve metals such as Ti-surface through utilizing electrolytic plasma during EPD process and finally improve adhesion properties of coatings [49–51]. Nevertheless, researches were mainly focusing on the deposition of continuous GO film on the PEO matrix, which totally cover the micro-nano pores. These approaches may devalue the initial benefit of the PEO porous structure, which is required to be present for bone-implant integration [22,48].

Motivated by these studies, we come up with a new concept to improve osseointegration and antibacterial properties of titania surfaces simultaneously by combining micro-nano porous PEO surface partially covered with GO, which is presented in this paper. To achieve this goal, a new fabrication strategy is introduced, which consists of two steps: initial fabrication of PEO titania substrate followed by its partial coverage with GO through PEO-EPD technique. We proposed that the partial GO deposition is critical to have a mixture of two types of surfaces, first- to improve osseointegration and secondly- to prevent bacterial adhesion and colonization. In this study, the effect of deposition time for the PEO-EPD process was explored to achieve the desired GO deposition pattern with partial surface coverage. The morphological, physiochemical, mineralization potential and antimicrobial characteristics of the deposited titania surfaces with optimized conditions are presented to evaluate their performances as a potential new surface engineering technology for biomedical implants.

2. Experimental section

2.1. Materials

Ti-foils with 99.9% purity and thickness of 1 mm provided by Nilaco (Japan); orthophosphoric acid (H_3PO_4), 85 wt%, potassium hydroxide (KOH) pellet, 30 wt% hydrogen peroxide (H_2O_2), sulphuric acid (H_2SO_4), 35 wt% hydrochloric acid (HCl) and ethylene glycol were obtained from Chem Supply (South Australia). Sodium metasilicate pentahydrate and potassium permanganate ($KMnO_4$) were supplied from Sigma-Aldrich Pty Ltd. and potassium fluoride (KF) from Ajax Sigma–Aldrich. Graphite powder with an average diameter of 250 μm was collected from Eyre Peninsula mining site, South Australia. Pure Milli-Q water was used with the resistivity of 18.2 MΩcm refined by EMD Millipore Corporation, Billerica machine.

2.2. Graphene oxide (GO) preparation

GO was prepared by chemical oxidation of graphite powder using modified Hummer's method [52]. In short, a 9:1 mixture of H_2SO_4 and H_3PO_4 was prepared and placed in a refrigerator to cool down to 3 °C. Then the acidic solution slowly added to the mixture of $KMnO_4$ (18 g) and graphite powder (3 g), while was stirred and heated up to 50 °C for about 13 h. After reaching the ambient temperature, 1 ml of H_2O_2 was gently added to the solution resulted in the formation of the brownish mixture. The solution was then centrifuged at 4200 rpm for 2 h with 35% HCl and distilled water, respectively.

2.3. Modification of titanium surface with plasma electrolytic oxidation (PEO) method

Samples with a specific size (2 cm × 1.5 cm) obtained from Ti-foils were cleaned by acetone in a sonication bath for 10 min followed by rinsing with DI water to remove any surface contamination. All samples were dried in the oven for 3 h at 50 °C. The programmable DC power supply (N5752A, Agilent Technologies, USA) was utilized for the anodization process, while voltage-time data were collected by coupled LabVIEW software. The PEO treatment was performed in a single step, under the galvano-static condition with a fixed current density of 50 mA/cm^2 and stirring speed of 250 rpm for 1 min by modifying previous research protocols carried out by Kuromoto et al. [53] and a similar basic electrolyte reported by Aliasghari et al. [53–55]. Briefly, the PEO electrolyte was comprised of sodium silicate, phosphoric acid as well as potassium hydroxide dissolved in deionized water. After PEO anodization treatment, samples were washed in an ultrasonic bath with Millipore water for 10 min and then dried in the oven for 2 h at 50 °C. The resulting coating was denoted as PEO sample.

2.4. Combined plasma electrolytic oxidation and electrophoretic deposition (PEO-EPD) for GO deposition

For the preparation of the GO solutions, 0.5 mg GO in the form of concentrated suspension was added to the 500 ml electrolyte containing ethylene glycol 94:5 wt%, deionized water 5 wt% and KF 0.5 wt% based on the modified research protocol by Ali et al. [56]. Prior to the PEO-EPD process, GO sheets in the electrolyte were dispersed by ultrasonic agitator for 20 min. The pH of solution and zeta potential of added GO were 12 and −29 mV, respectively. The PEO-EPD process was carried out in different deposition time (7, 15, 30 and 60 s) without electrolyte agitation under the constant current mode of 100 mA/cm^2 using two-electrodes cell arrangement with working electrodes distance of 13 mm. The working electrode was PEO substrate and the counter electrode was a Ti-plate which situated parallel facing each other. The coated samples were removed from the cell and dried in an electric oven for 2 h at 50 °C.

3. Characterizations

Structural characterization of the porous structure obtained from PEO treatment and GO-enhanced morphology were investigated by SEM Quanta 450 (field emission scanning electron microscope, Eindhoven) coupled with EDS analysis as well as FIB-SEM (Focused Ion Beam Scanning Electron Microscope FEI Helios Nanolab 600, USA). The Zeta potential measurement of the electrolyte containing GO was carried out utilizing Malvern Zetasizer Nano Series (NS) before the deposition process. Surface topography of samples and surface roughness analysis were performed using a benchtop 3D optical profiler (Bruker ContourGT-K1). The vertical scanning interferometry (VSI) mode with a 20× objective was utilized for profilometry analysis. Raman spectroscopy instrument (WITEC Alpha300) was exploited to analyze the oxide layer after PEO process and to confirm the presence of GO after deposition process (PEO-EPD) with the range of 0–2000 cm^{-1} wavelength with a 532 nm laser beam. XRD analysis was carried out employing Rigaku MiniFlex 600, with the operating condition of (40 kV, 2θ = 3–80 with a scan rate of 2.5). Contact angle measurement was performed using optical-tensiometers model T301 – ATA scientific pty ltd and sessile drop method with droplet size of, 2.2 ± 0.1 μl. Microhardness test was also performed using a microhardness tester (ECO LM700, USA) with the predefined condition of 100 g force and dwell time of 10 s, which was applied over the surface of samples. The biomineralization test was performed according to the literature reported by Kokubo et al. [57]. In brief, samples were immersed in 50 ml simulated body fluid (SBF) solution for 21 days, while the solution was being replaced every two days to maintain the level of ion concentrations adequate for mineralization process. The antibacterial test was conducted according to ISO 22916:2011 against *E. coli* (Gram-negative, DSM 3423) and *S. aureus* (Gram-positive, DSM 346) bacteria. Briefly, bacteria were grown overnight and next diluted to a final concentration of 6×10^5 Colony Forming Unit (CFU)/ml to be inoculated (12.6 μl) on the surface of UV-disinfected (20 min per side) test specimens of about 10 mm × 10 mm. In order to obtain a homogeneous layer of bacteria, polypropylene coverslips (8 mm in diameter) were placed on the top of test inoculum, and the samples were incubated for 24 h at 37 °C in a humidified atmosphere. Bacteria were then eluted, serially diluted, and plated on Petri dishes containing agar growth medium and cultured for another 24 h at 37 °C. CFUs were finally counted and the antibacterial activity was calculated according to the following:

$$I\,(\%) = \frac{B_{CTRL} - B_{test}}{B_{test}} * 100$$

Where I (%) is the percentage of bacterial inhibition, B_{CTRL} is the viable bacteria recovered from control samples (untreated Ti), B_{test} is the viable bacteria recovered from specific samples. Samples were tested at least in triplicate, and related data were stated as the mean ± standard deviation and were analysed using GraphPad version 6 software (GraphPad Software, La Jolla, CA). Statistical comparison among groups was performed via one-way analysis of variance (ANOVA) (multiple comparisons) with post hoc Tukey's test to indicate significant differences between experimental groups. Differences were considered statistically significant when $P < 0.05$.

4. Results and discussions

4.1. Voltage–time response of PEO process and morphological characteristics of fabricated PEO titania structures

The basic solution for the PEO process is selected in this work, as it is more effective than the acidic electrolyte for the fabrication of protective and robust oxide layers [53,55]. Moreover, our previous research showed that 1 min PEO treatment is the optimized duration to achieve a suitable voltage for the fabrication of micro-nano structured pores, which can cover the entire surface with the desired morphology. Further PEO treatment would only increase the oxide layer thickness and does not affect the overall morphology required for the osseointegration improvement. Typical voltage–time (V-t) response curve for the PEO treatment in the basic electrolyte was generated by LabVIEW software, using single-step anodization at 50 mA/cm^2 and provided in Fig. 1a. The result showed an increasing trend in the cell voltage values with a breakdown voltage of ~310 V after 40 s, which was evident by the formation of arcs starting from the edge of the sample. Moreover, at around 60 s, voltage reached to ~380 V, arcs became brighter and spread all over the working electrode. Finally, the PEO process led to the formation of a generic porous micro-nano structure on Ti sample similar to the PEO surface morphology reported by Aliasghari et al. [55]. Fig. 1b shows the SEM image of the substrate after the PEO process. The formed oxide layer was enriched with silicon and titanium (supplementary Fig. S1), comprised of pores ranging from 200 nm to 1 μm with an

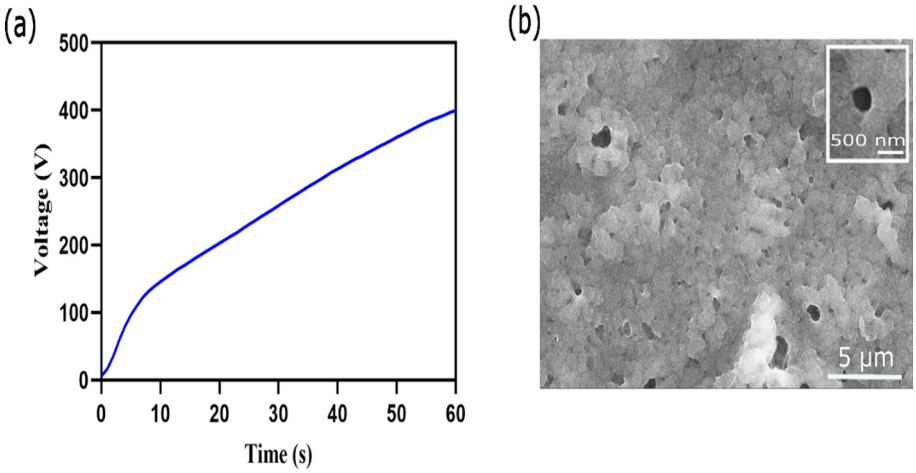

Fig. 1. a) Voltage-Time plot for the PEO process, b) SEM image of fabricated PEO titania surface with PEO technique in the basic solution at 50 mA/cm^2 after 1 min.

average spacing of 1.62 μm (between bigger pores) and few crater-like morphologies, which were distributed along the flat oxide layer surface. This analysis was taken from at least 15 spots with "Image J" software. A typical single pore morphology after PEO process is presented on the inset of Fig. 1b.

Overall, these results confirm the successful formation of PEO porous micro-nano morphology over the Ti substrate. Similar researches have shown the ability of these modified surfaces to promote osseointegration via increasing the surface area and attachments sites between bone cells and the implant surface [58,59].

4.2. Voltage–time response of PEO-EPD process for GO deposition and morphological characteristics of PEO-GO surface

Deposition of GO on PEO surface was performed in the next step using PEO-EPD process. Fig. 2 summarizes the voltage–time response and optical microscopy images of the generated PEO-GO surface after deposition at different durations. Fig. 2a shows a sudden increase of voltage to 455 V followed by a sharp decrease to ~320 V and a subsequent gradual decrease to reach a stable value of ~230 V for 1 min of the deposition process. It is important to note that, the proposed GO

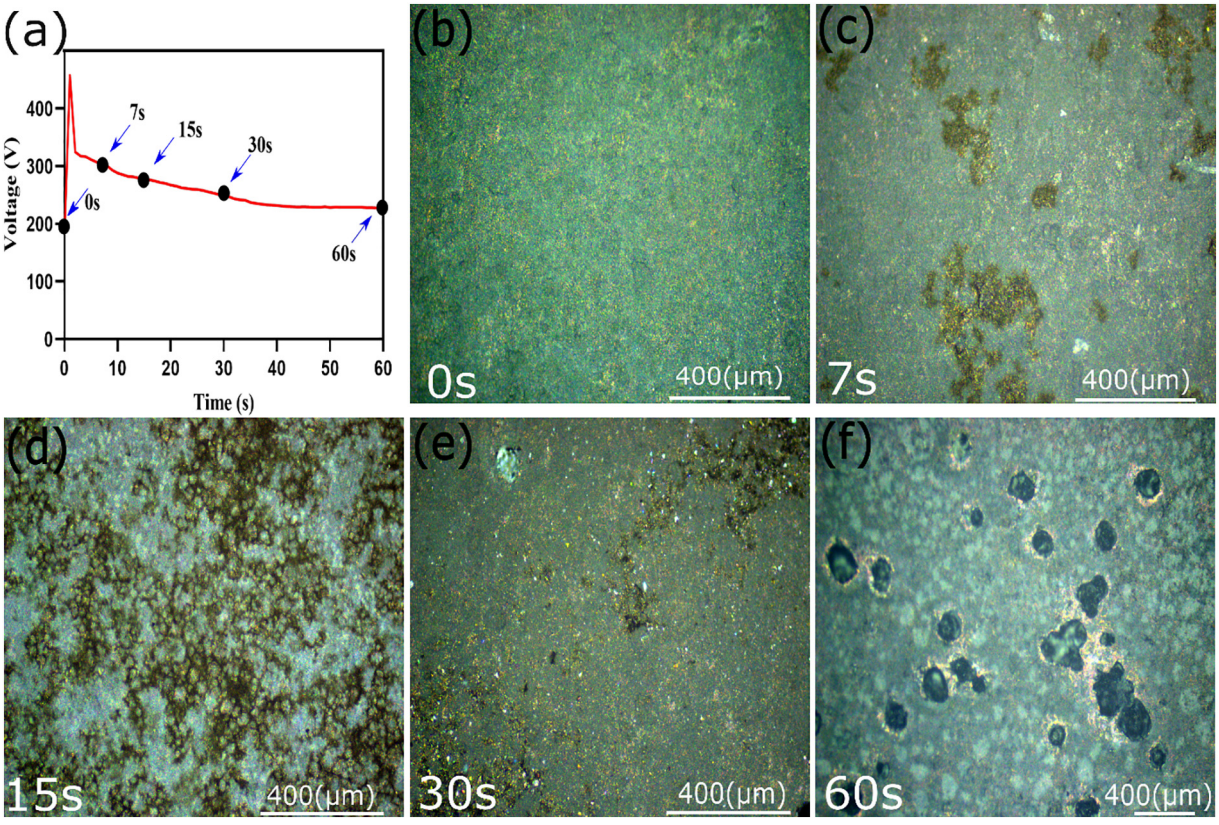

Fig. 2. a) Voltage-time plot during PEO-EPD process for deposition of GO on PEO surface. Optical images of PEO-GO surface obtained by PEO-EPD process during the different time: b) 0 s (PEO control), c) 7 s (EPD-7), d) 15 s (EPD-15), e) 30 s (EPD-30) and f) 60 s (EPD-60) showing the different density of GO patches on PEO titania surface.

deposition method with PEO-EPD technique in this study, doesn't follow the typical EPD kinetics described by Hamaker's law [46]. This deviation from linearity is mainly attributed to the generation of gases, secondary PEO arcs and thickening of GO insulating layers at high voltage EPD process (PEO-EPD) [60]. Fig. 2 represents the optical images of GO deposition pattern with PEO-EPD process at 0, 7, 15, 30 and 60 s, which are denoted as EPD-0 (PEO control sample), EPD-7, EPD-15, EPD-30 and EPD-60, respectively.

Organic electrolyte (ethylene glycol) is known to help to reduce the gas formation during high voltage EPD process. However, a small addition of water is added to the electrolyte to generate micron-sized bubbles through hydrolysis at electrodes. These formed bubbles along with the secondary arc generation during high voltage EPD process would provide better control for deposition of GO patches with the desired coverage [60]. During PEO-EPD process, negatively charged GO flakes in the electrolyte were attracted to the PEO substrate (positive pole) driven by the electric force. Then, the deposition took place on the working electrode gradually. Fig. 2b shows the PEO control surface before GO deposition (EPD-0), while the deposition pattern after 7 s (EPD-7) is presented in Fig. 2c. By increasing the deposition time to 15 s, the formation of small bubbles partially impedes the attachment of GO flakes, while deposition continues to take place in the other zones. The most uniform pattern of GO deposition is presented in Fig. 2d, achievable within 15 s of the deposition process (EPD-15) that is accepted as optimal surface and condition. As previously mentioned, another factor involves in the current PEO-EPD process is "the secondary arc generation". Due to the sudden jump of cell voltage to over 400 V, as a result of alternative PEO process, secondary arcs were generated, which bombarded the surface and gradually disrupted the uniform deposition process. Here, after 30 s of PEO-EPD process, the formation of secondary arcs and gases, known as "high voltage EPD side reactions" [60] were intensified and resulted in the disruption of GO deposition process and formation of large-sized pores (Fig. 2e). Finally, after 1 min of PEO-EPD process, strong arcs and intensive gas formation completely ruined the coating and they left the surface with very large-sized holes (>200 μm diameter, evident in Fig. 2f).

To further reveal surface morphology and chemical composition of optimized PEO-GO substrate prepared by 15 s of PEO-EPD process, series of SEM and EDS images are presented in Fig. 3. Fig. 3a and b clearly show the presence of GO flakes on the blurry and dim zones of the image that partially are covering the PEO porous structure. Moreover, many open pores are still detectable in the image. Fig. 3c represents the FIB-SEM cross-section image of the sample from a random site with GO presence. As can be seen, the average PEO thickness is around 800 nm (EDS mapping of the cross-section also has been provided in the supplementary Fig. S4). EDS analysis confirmed the presence of C with more than 28 wt% in the cross-section (Fig. 3d). SEM images showed the presence of PEO pores ranging from 50 nm to 1 μm with an average spacing of 1.02 μm between the bigger pores. Moreover, the result of Raman intensity mapping of GO for 100 μm ×100 μm area of PEO-GO sample with steps of 10 μm (Fig. 3e) showed GO sheets covered around 66% of the PEO substrate (also supplementary Fig. S2). Further pixel analysis of PEO-GO optical image with Image J software in Fig. 3f confirmed more than 57% of the surface was covered with GO (supplementary Fig. S3 and Table S1 for the pixel density calculation).

The results of surface topography and comparative surface profile analysis are presented in Fig. 4. Both 2 D and 3 D images for PEO surface before GO deposition (EPD-0) demonstrated the inhomogeneous presence of pores along the surface (Fig. 4a), while after GO deposition for 15 s (PEO-GO) many of these pores were covered with GO layers and a reduced number of pores was observable (Fig. 4b). On the other side, analysis of topography profile of surfaces in Fig. 4a and b revealed a significant increase of profile height both in X and Y directions as a result of further PEO treatment during PEO-EPD process. Moreover, the profile of the PEO surface was characterized by the arithmetic mean of profile roughness (Ra), root-mean square of profile roughness (Rq), and total height roughness (Rt) of 0.65, 0.83 and 4.82 μm, respectively. Whereas, for coated GO samples, these numbers were remarkably increased to 0.85, 1.05 and 6.69 μm correspondingly.

4.3. Compositional and mechanical characterization of fabricated PEO substrate decorated with GO (PEO-GO)

The XRD spectra for PEO (control) and PEO-GO after GO deposition for 15 s with PEO-EPD process (EPD-15) is depicted in Fig. 5a. Comparison between XRD patterns of standard peaks for anatase phase (JCPDS card No. 21–1272) and titanium standard (reproduced by JCPDS card, no. 65–3362) is confirming the formation of anatase on both PEO and PEO-GO samples. Particularly, diffraction peaks at 2θ values of 25.8°, 39.1° and 48.5° can be indexed to the (101), (112), and (200) planes of the anatase phase. These results are also consistent with the previous PEO surface XRD spectra analysis reported by Malinovschi et al. [61]. Moreover, a small shift towards the left side of the XRD spectra noticed after PEO-EPD process. Based on the literature, the observed shift towards lower 2θ values in the XRD spectra is associated with the expansion of TiO_2 lattice, which probably occurs during the high voltage PEO-EPD process [62].

It is worth mentioning that when the cell voltage during PEO treatment exceeds the breakdown voltage of the oxide layer, thousands of micro arcs are formed and hit the titanium surface.

These micro-arc discharges can increase the temperate to more than 4500 K and lead to local melting of the Ti outer surface [63]. The presence of electrolyte in the system would result in the rapid cooling of the surface in a very short period and favours the development of anatase and rutile phases [61]. Different studies suggested that the anatase phase is more beneficial for nucleation of HAp on Ti surface when it is compared to rutile phase [64]. As a result, it is expected that both PEO and PEO-EPD samples, which demonstrated anatase peaks in their XRD spectra would have suitable osseointegration properties.

On the other side, XRD spectroscopy is considered as a bulk analysis technique. Consequently, it is not able to reveal the corresponding feature peak for GO at 11° on the surface of the GO coated PEO substrate [65]. Therefore, other spectroscopy techniques such as Raman Spectroscopy is required to confirm the presence of GO over the surface.

To identify the presence of GO, Raman spectroscopy was utilized before and after GO deposition process (Fig. 5b). PEO substrate before PEO-EPD process is characterized with 4 peaks obtained at ~146, 390, 514 and 628 cm^{-1}, which were associated with the formation of the anatase phase over the oxide layer. The Raman spectrum of the PEO-GO confirmed the presence of two distinguished peaks at 1341 cm^{-1} and 1590 cm^{-1}, known as D and G bands for GO, respectively [66]. These peaks exhibit the successful introduction of GO to the PEO surface. The I_D/I_G value is known as "Intensity ratio" calculated after GO deposition is around 1.04, which is in the range of reported values in other similar experiments [67]. In general, G band is associated with phonon scattering from sp^2 C atoms that lays in range of ~1500–1600 cm^{-1}, while D peak confirms the presence of defects, impurities and disorientation in sp^3 bonded C atoms that change in the range of ~1200–1500 cm^{-1} [68]. Meanwhile, no peak was observable for Ti strip sample before the PEO process.

Measured contact angle (CA) values for pure titanium control sample as well as PEO and PEO-GO (EPD-15) are presented in Fig. 5c. In this experiment, Ti sample showedCA ~74°, while PEO control demonstrated better hydrophilicity as a result of engineered micro-nano structure introduced to the surface via PEO process (CA~ 63°). Moreover, After GO deposition, due to the presence of GO and the formation of bigger pores during PEO-EPD process, CA value dropped drastically to around 16°. The measured CA values for PEO (CA~63°) and PEO-GO (CA~16°) samples in this work are consistent with previous results for PEO (with CA~ 60°) and PEO covered with GO thin film (with CA~ 19°) reported in the similar study [22]. It is worth mentioning that high wettability of implant surface, plays an essential role in bone

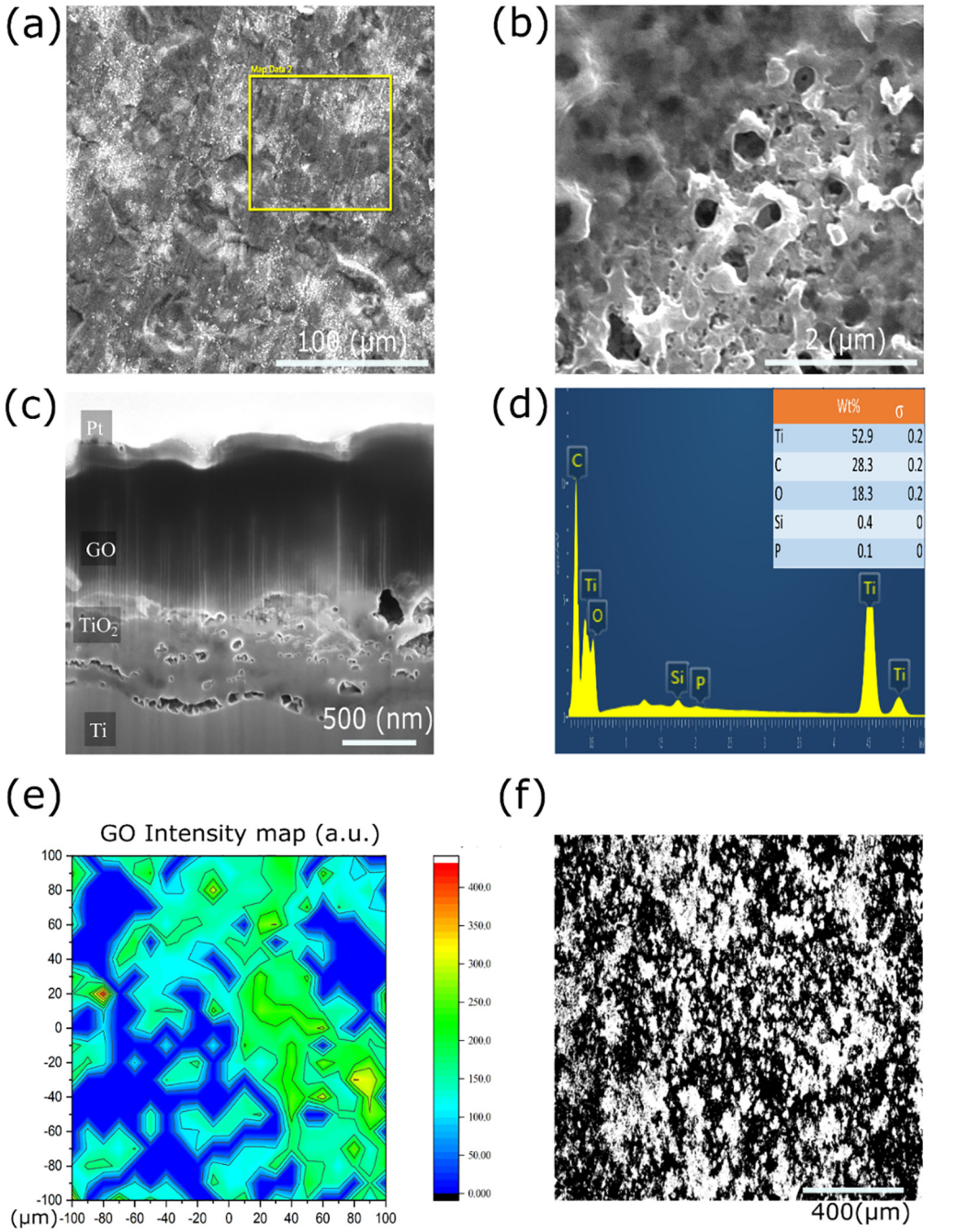

Fig. 3. SEM image of optimized PEO-GO sample (EPD-15) at a) low magnification, b) high magnification, c) PEO-GO sample cross-section, d) EDS results from PEO-GO cross-section, e) Raman GO intensity mapping of PEO-GO for 100 μm × 100 μm area, f) Converted PEO-GO (EPD-15) optical image to black-white colour for GO concentration calculation with Image J.

bonding and bioactivity of titanium bone implants [69,70]. Similar research conducted on a PEO sample covered with GO thin film with low CA values reported a dramatic increase in the proliferation and osseointegration abilities of the surface. Therefore, the fabricated PEO-GO samples in the current work with relatively high wettability are also expected to promote cell adhesion and proliferation [22].

The results obtained by Vickers micro-hardness test from PEO and PEO-GO substrates have been presented in Fig. 5d. The microhardness values for untreated Ti sample also have been provided for comparison. It is evident that PEO modification has improved the mechanical hardness of the Ti sample from 141 Hv to 154 Hv. The formation of anatase during PEO treatment can justify this outcome, wherein the presence of the oxide layer has been confirmed by XRD and Raman spectroscopy. Previous research reports also suggested that the formation of anatase can improve the micro-hardness of the PEO coatings [40,71]. After PEO-EPD treatment and GO deposition (EPD-15), hardness value depicts a further increase to ~171 Hv. A possible explanation for the observed results would be the generation of the secondary arcs during PEO-EPD process, which gives extra mechanical strength to the oxide layer [50,72]. It's well known that the increase in the PEO treatment duration results in the thickening of the oxide layer. As a result, the mechanical hardness of the coating is improved [73]. However, the lower

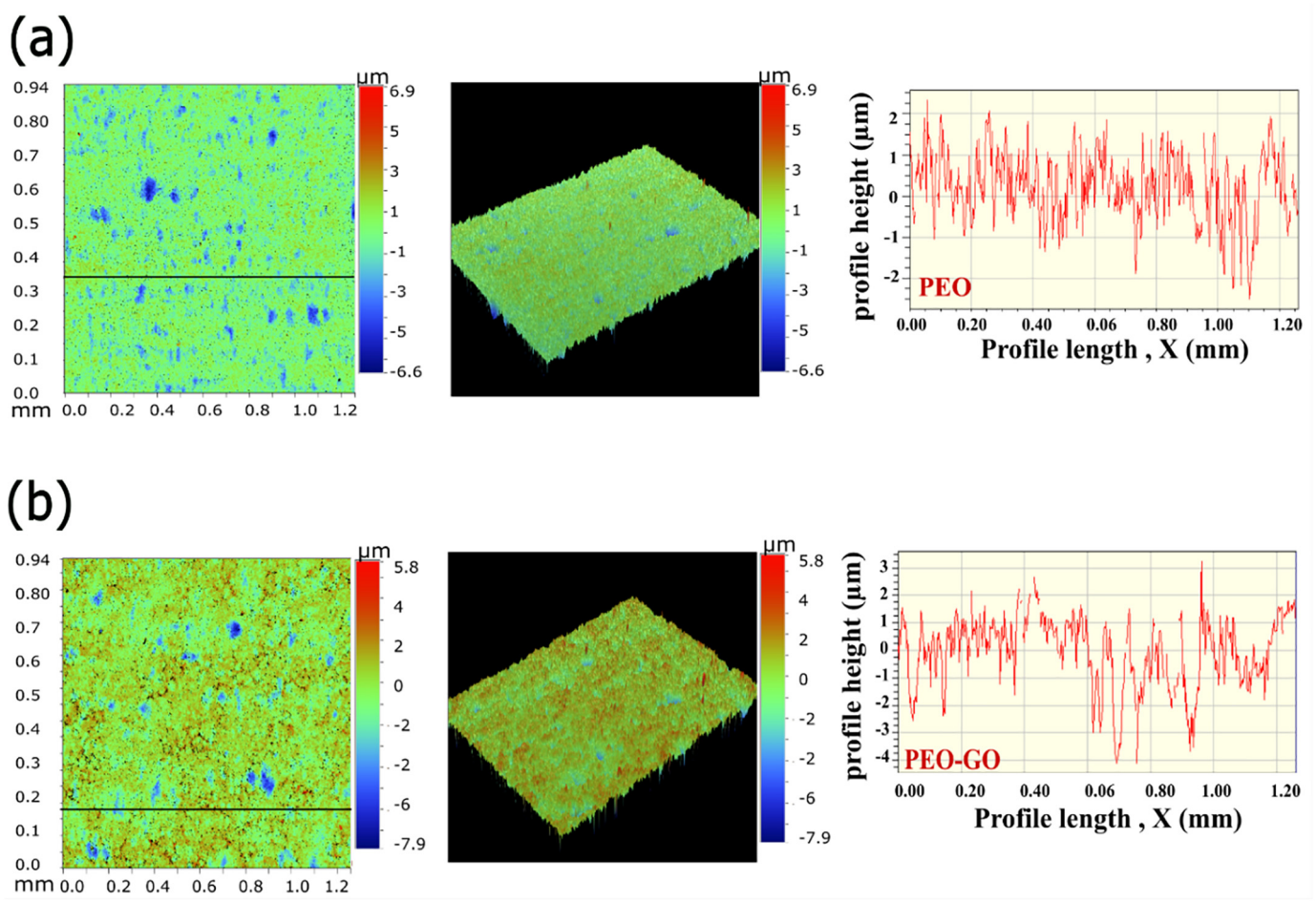

Fig. 4. Comparative image of 2D and 3D images and cross-sectional surface profile graphs of PEO and PEO-GO surface obtained by optical profilometry: a) Surface morphology of PEO sample (EPD-0), b) Surface morphology of PEO-GO sample (EPD-15).

electrical conductivity of the oxide layer on the PEO substrate would interfere with the successful deposition of GO sheets on the PEO substrate in the subsequent PEO-EPD process. For that reason, the initial PEO process in this research only performed for one 1 min to form a thin oxide layer with around 800 nm thickness. This PEO duration guaranteed the total coverage of Ti-surface with the desired micro-nano morphology required for the osseointegration improvement. The thinner PEO oxide layer thickness on our samples explains the observed lower microhardness values for the fabricated samples compared to the previous studies [61,74]. Finally, no vulnerability to brittle fracture observed over both treated samples which signifies strong bonding between the oxide layer and Ti substrate.

4.4. Bio-mineralization test

SEM, XRD and EDS analysis of PEO control (EPD-0) and GO modified sample, PEO-GO, after 21 days immersion in SBF solution are presented in Fig. 6. The SEM result showed the formation of small particles around 1.4 μm over the PEO-GO/SBF surface. The PEO control surface after SBF immersion (PEO/SBF) also showed smaller particles, which were deposited over the surface. XRD spectra of both PEO and PEO-GO samples after immersion showed some of the main characteristic peaks of hydroxyapatite corresponding to (100), (200), (002), (102), (112), (300), (301), (312) and (231) planes (based on ICDD 9–432 [75]), which are confirming the presence of HAp along with other salts on both PEO and PEO-GO samples after SBF immersion. Magnified XRD pattern of samples after mineralization are presented in the supplementary section, Fig. S5.

EDS analyses are also performed and their results confirmed the presence of Ca and P on both PEO and PEO-GO samples (with Ca/P molar ratio more than 2) after biomineralization test (Fig. 6d and e). Based on previous research, when Ca/P ratio is greater than 1.667, the mineralized materials form a biphasic mixture comprised of calcium phosphate apatite and $Ca(OH)_2$ [76]. It is worth mentioning that while appetite formation was evident on both treated samples after SBF test, no mineralization observed for Ti sample. The SBF is comprised of chemicals similar to the human plasma and the SBF mineralization test is considered as a powerful method to predict the in-vivo bioactivity of implant surface [77]. Therefore, the growth of apatite on both PEO and PEO-GO samples after immersion in SBF demonstrates their possible ability to improve osseointegration through the formation of interfacial bonds between bone cells and implant surface after implantation [78].

4.5. Antibacterial activity characterizations

The optical images of bacterial colonies on Petri dishes after recovery from PEO and PEO-GO substrates and further cultivation are presented in Figs. 7a–f. From photographs, it is apparent that the number of colonies for both *E. coli* and *S. aureus* bacteria is substantially decreased after direct contact with GO-deposited substrates (EPD-15). Particularly *S. aureus* cell growth was completely inhibited on PEO-GO surface, which implies that the substrate displays a high antibacterial activity

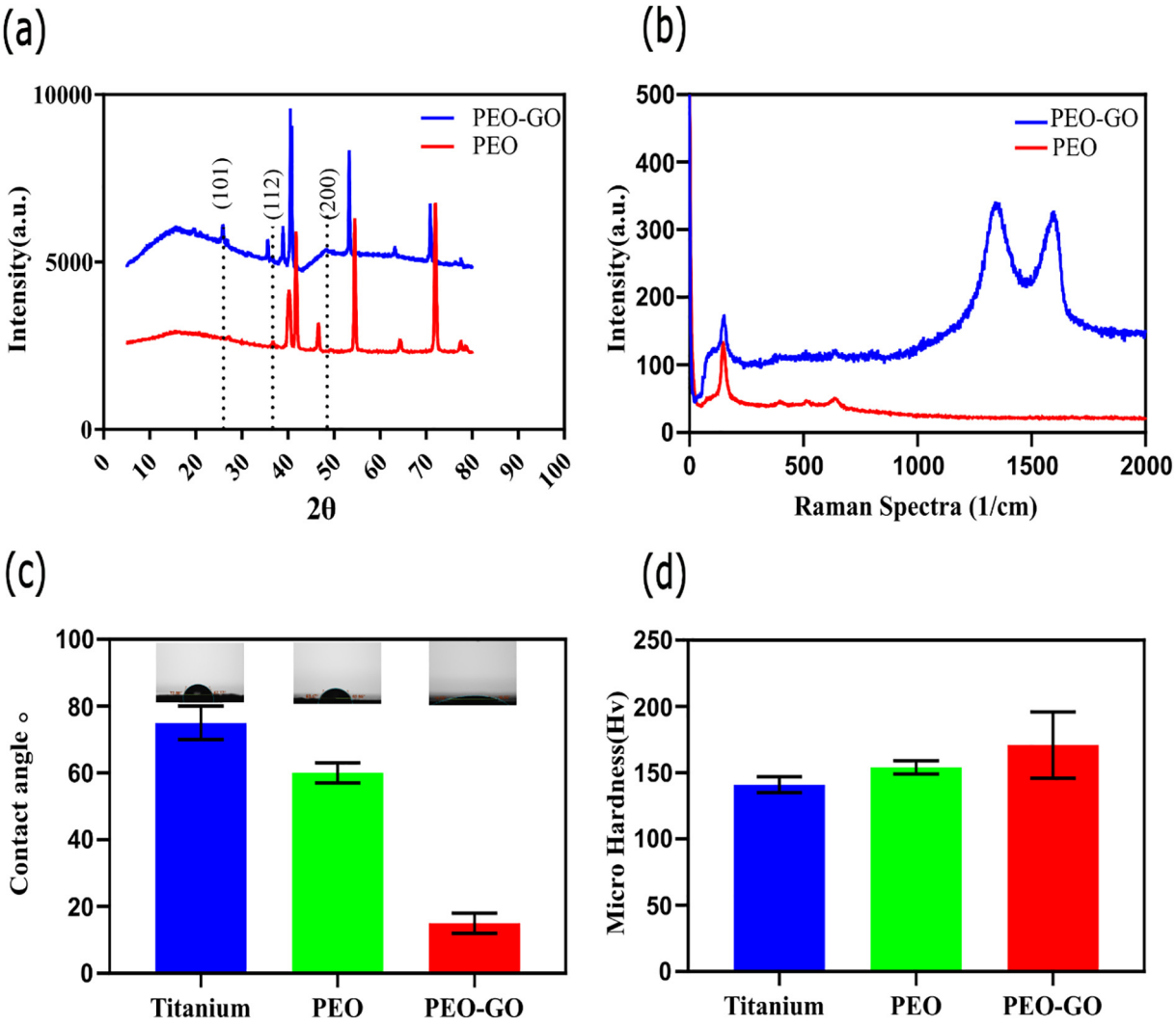

Fig. 5. Comparative chemical, mechanical, interfacial, and surface analysis of PEO control (EPD-0) and PEO-GO (EPD-15) after GO deposition: a) XRD graphs, b) Raman graphs, c) Contact angle measurement, d) Micro hardness test.

against this bacterium. A relative bacteria cell viability over different samples are reported in Fig. 7g and h. These results showed no notable antimicrobial activity for CTRL samples (Ti), while PEO-GO substrates did inactivate 79(±11)% of *E. coli* bacteria ($p<0.01$). Moreover, as mentioned above, no viable *S. aureus* was eluted from PEO-GO ($p<0.01$), which demonstrates a high vulnerability of *S. aureus* bacteria to the GO deposited substrate. On the other hand, PEO substrate showed some extent of antibacterial activity against *S. aureus* (I (%) = 52(± 17)%, $p<0.05$), while no effect was found against *E. coli*. Similar studies on the antibacterial assessment of modified PEO samples also point out that the modified PEO samples may only show the antibacterial activity against a particular type of bacteria, while they can be ineffective against other types of bacteria [79]. Moreover, the higher sensitivity of gram-positive bacteria such as *S. aureus* to the GO coated surface compared with *E. coli* bacterium was also reported by Akhavan et al. [80]. The plausible explanation for higher resistance of *E. coli* bacteria against mechanical damage induced by GO sheets could be attributed to the presence of a protective outer membrane in gram-negative *E. coli* bacteria. This membrane is instead absent in gram-positive *S. aureus* bacteria. This could make gram-positive bacteria more vulnerable to direct contact interaction with GO sheets [80]. Based on the literature data, GO sheets demonstrate high antibacterial ability against different types of bacteria such as *E. coli, S. aureus and P. aeruginosa* [81,82]. Recently, Sun et al. [22] reported a similar antibacterial activity for GO coated PEO samples against *S. mutans* with a high antibacterial ratio of 90.81%. This finding also highlights the superior antibacterial ability of GO/PEO mixture against gram-positive bacteria. Among different proposed mechanisms associated with the antimicrobial ability of GO, mechanical damage of bacteria membrane via direct contact with GO sharp edges and the generation of reactive oxygen species triggered by GO oxidative stress and charge transfer are more plausible scenarios [83,84]. Overall, the fabricated PEO-GO samples in this work demonstrated a very high antibacterial activity against *E. coli* and *S. aureus* bacteria, which makes the PEO-EPD process a suitable approach for fabrication of the next generation of antimicrobial GO-coated implants.

5. Conclusion

In summary, the fabrication of PEO titania surface with partially decorated GO sheets was achieved by combined PEO-EPD process. The optimization of PEO-EPD process was carried out in different time interval between 0 s to 1 min, showing the most desirable coverage of GO at 15 s (sample EPD-15), which was confirmed with optical microscopy and optical profilometry. Raman spectroscopy showed the presence of D and G bands, confirming the deposition of GO over the PEO matrix. XRD analysis demonstrated the formation of anatase titania phase

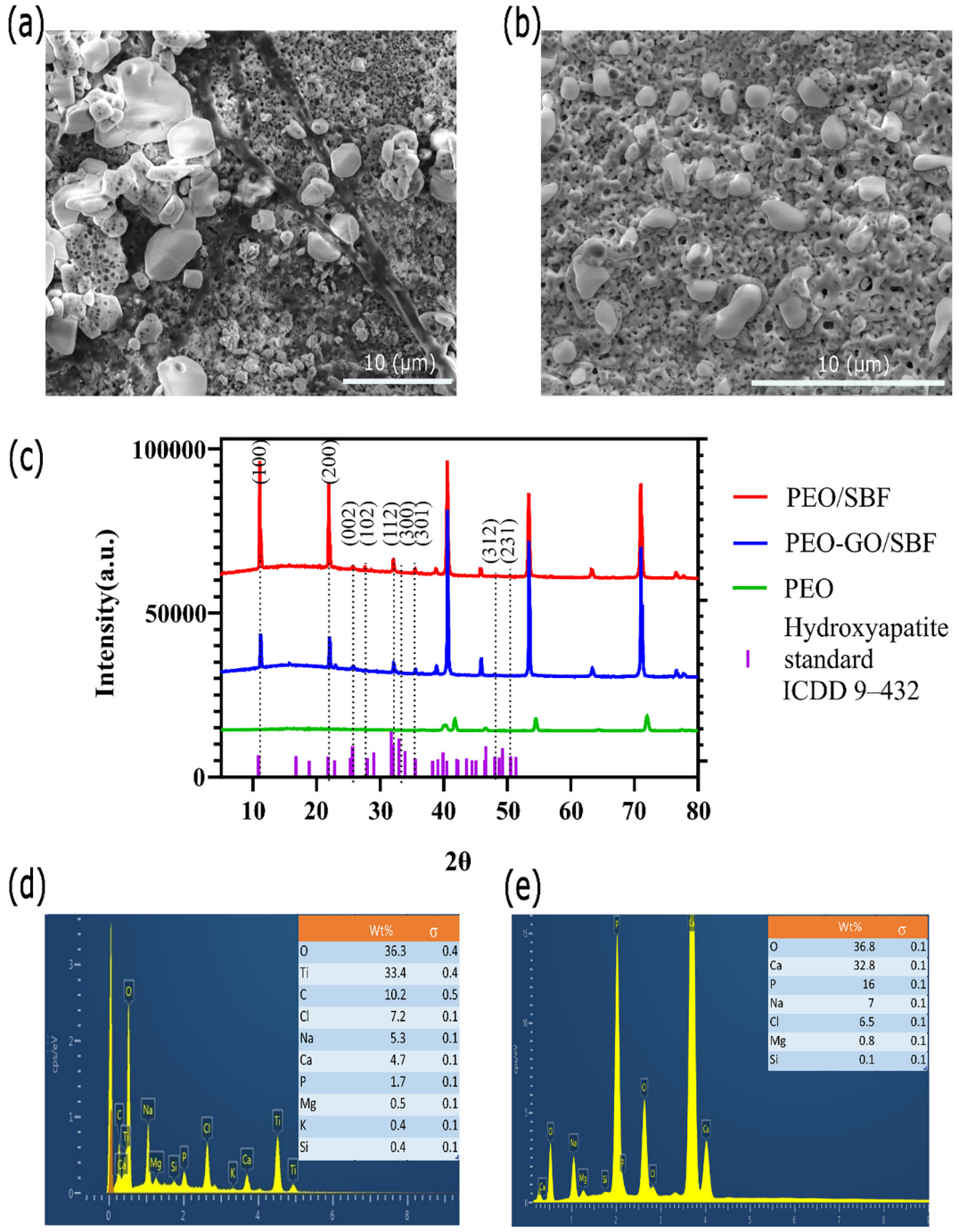

Fig. 6. SEM image of samples after SBF test: a) PEO-GO, b) PEO), c) XRD spectra of different samples before and after SBF mineralization test, d) corresponding EDS analysis for PEO-GO/SBF, e) corresponding EDS analysis for PEO/SBF.

after the PEO treatment. Vickers hardness test showed an improvement in hardness of the coating after PEO and a further increase of hardness values after PEO-EPD treatment with 154 Hv and 171 Hv, respectively. The calculated hardness values for bare titanium surface was around ~141 Hv. Moreover, CA measurements showed a notable decrease in values to ~16° after PEO-EPD treatment. SBF mineralization test carried out and confirmed the presence of HAp on both PEO and GO coated PEO samples. The antibacterial study showed significant antibacterial activity of GO decorated PEO surface for both bacteria compared to control, with the antibacterial rate of ~80% for *E.coli* and ~100% for *S.aureus*. In short, PEO-EPD process showed a significant potential for fabrication of controllable GO coating on the PEO titania substrate. This can address both osseointegration and antimicrobial performance of the titanium implants and open a new door in the application of graphene derivatives in bone-implant industries.

Author statement

Arash Mazinani: most investigation, methodology data processing, writing first draft

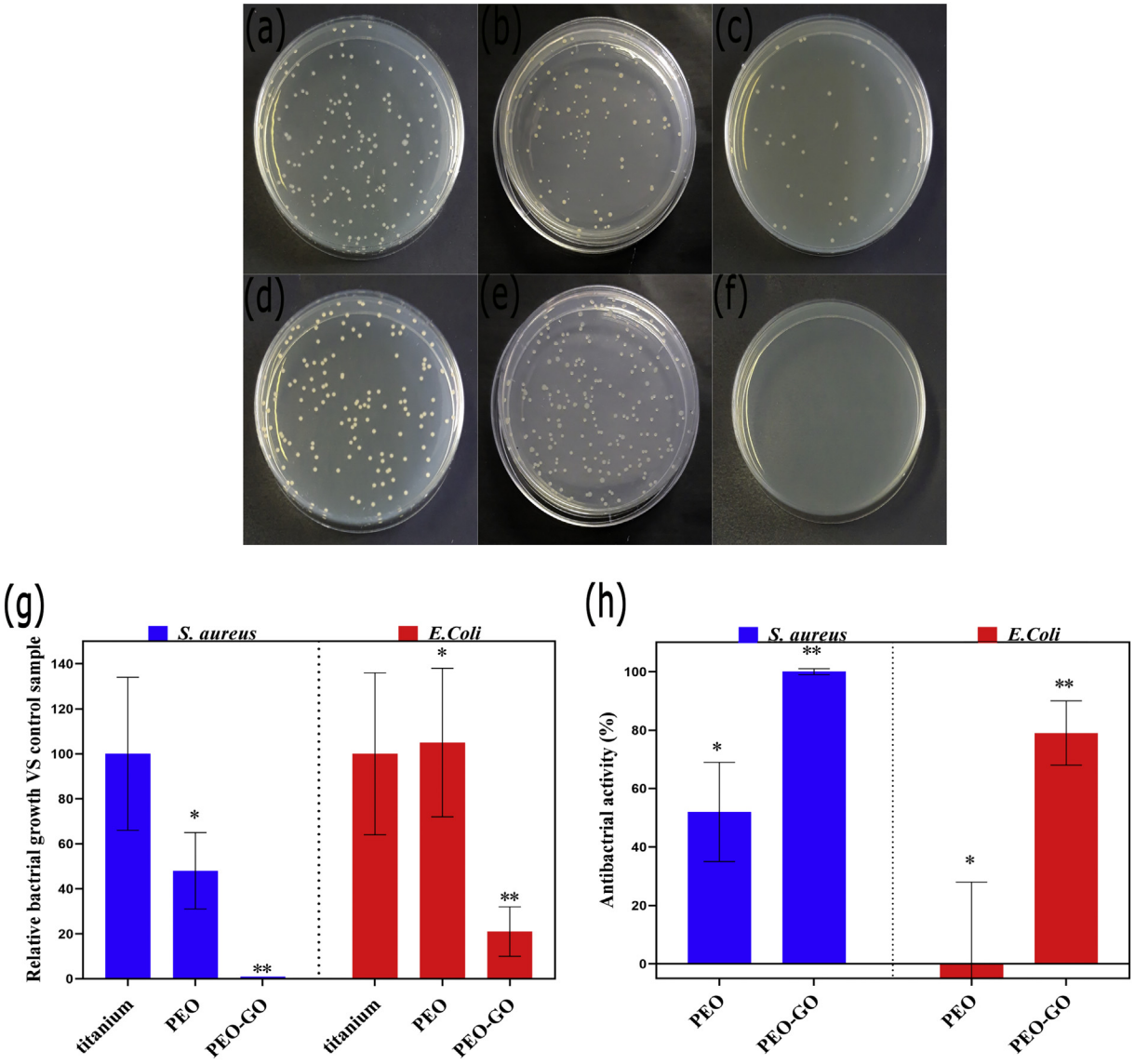

Fig. 7. Analysis of bacterial viability on control, PEO and PEO-GO (EPD-15) substrates. Photographs of *E. coli* colonies on agar Petri dishes after elution from: a) CTRL (Titanium) sample, b) PEO, c) PEO-GO substrate; photographs of *S. aureus* colonies after elution from d) CTRL (Ti) sample, e) PEO, f) PEO-GO substrate; g) relative bacterial growth in contact with different samples; h) corresponding antibacterial activity of different samples. $^{*}p < 0.05$; $^{**}p < 0.01$ vs. control.

Md Julker Nine: co-supervisor, methodology, some data processing, Review & Editing

Roberto Chiesa: bacterial study, Review & Editing

Gabriele Candiani: bacterial study, Review & Editing

Paolo Tarsini: bacterial study, Review & Editing

Tran Thanh Tung: some data processing, Review & Editing

Dusan Losic: principal supervisor, Review & Editing, Resources, Submission

Declaration of Competing Interest

There are no conflicts to declare.

Acknowledgements

The authors acknowledge the funding by the ARC Research Hub for Graphene Enabled Industry Transformation, (IH150100003). The authors thank the University of Adelaide, school of chemical engineering and advanced materials and department of chemistry, materials and chemical engineering "G. Natta", Polytechnic University of Milan and Professor Reza Ghomashchi for their support in this project.

Appendix A. Supplementary data

Supplementary data to this article can be found online at https://doi.org/10.1016/j.matdes.2020.109443.

References

[1] L. De Nardo, et al., Electrochemical surface modifications of titanium and titanium alloys for biomedical applications. Coatings for Biomedical Applications, Woodhead Publishing, 2012 106–142.
[2] C.N. Elias, et al., Biomedical applications of titanium and its alloys, JOM 60 (3) (2008) 46–49.
[3] S. Maher, et al., Engineered titanium implants for localized drug delivery: recent advances and perspectives of Titania nanotubes arrays, Expert Opinion on Drug Delivery 15 (10) (2018) 1021–1037.
[4] V.D. Bui, et al., Antibacterial coating of Ti-6Al-4V surfaces using silver nano-powder mixed electrical discharge machining, Surf. Coat. Technol. 383 (2020), 125254.
[5] T. Albrektsson, et al., Osseointegrated titanium implants. Requirements for ensuring a long-lasting, direct bone-to-implant anchorage in man, Acta Orthop. Scand. 52 (2) (1981) 155–170.
[6] B. Klinge, et al., Peri-implant diseases, Eur. J. Oral Sci. 126 (S1) (2018) 88–94.
[7] T. Hanawa, Titanium–Tissue Interface Reaction and Its Control With Surface Treatment, Front. Bioeng. Biotechnol. 7 (170) (2019).
[8] E. Marin, et al., Effect of etching on the composition and structure of anodic spark deposition films on titanium, Mater. Des. 108 (2016) 77–85.
[9] E. Farber, et al., Development of the titanium meshes by selective laser melting and chemical etching for using as medical implants, Materials Today: Proceedings 30 (2020) 746–751.
[10] J.C.M. Souza, et al., Nano-scale modification of titanium implant surfaces to enhance osseointegration, Acta Biomater. 94 (2019) 112–131.
[11] C. Hallgren, et al., An in vivo study of bone response to implants topographically modified by laser micromachining, Biomaterials 24 (5) (2003) 701–710.
[12] D. Losic, et al., Titania nanotube arrays for local drug delivery: recent advances and perspectives, Expert Opin. Drug Delivery 12 (1) (2015) 103–127.
[13] E. Al-Hassani, F. Al-Hassani, M. Najim, Effect of polymer coating on the osseointegration of CP-Ti dental implant, 1968, 2018 030022 1.
[14] M. Montazeri, et al., Investigation of the voltage and time effects on the formation of hydroxyapatite-containing titania prepared by plasma electrolytic oxidation on Ti–6Al–4V alloy and its corrosion behavior, Appl. Surf. Sci. 257 (16) (2011) 7268–7275.
[15] I.d.S.V. Marques, et al., Biomimetic coatings enhance tribocorrosion behavior and cell responses of commercially pure titanium surfaces, Biointerphases 11 (3) (2016), 031008.
[16] S. Yang, et al., Hydrothermal treatment of Ti surface to enhance the formation of low crystalline hydroxyl carbonate apatite, Biomater. Res. 19 (2015) 4–6.
[17] E. Sandrini, et al., In vitro assessment of the osteointegrative potential of a novel multiphase anodic spark deposition coating for orthopaedic and dental implants, J. Biomed. Mater. Res. B Appl. Biomater. 73 (2) (2005) 392–399.
[18] W. Mu, Y. Han, Characterization and properties of the MgF2/ZrO2 composite coatings on magnesium prepared by micro-arc oxidation, Surf. Coat. Technol. 202 (17) (2008) 4278–4284.
[19] L. Snizhko, et al., Anodic processes in plasma electrolytic oxidation of aluminium in alkaline solutions, Electrochim. Acta 49 (13) (2004) 2085–2095.
[20] D.V. Mashtalyar, et al., Hard wearproof PEO-coatings formed on Mg alloy using TiN nanoparticles, Appl. Surf. Sci. 503 (2020), 144062.
[21] S.V. Gnedenkov, et al., Formation and properties of composite coatings on aluminum alloys, Russ. J. Inorg. Chem. 62 (1) (2017) 1–11.
[22] N. Sun, et al., Graphene oxide-coated porous titanium for pulp sealing: an antibacterial and dentino-inductive restorative material, J. Mater. Chem. B 8 (26) (2020) 5606–5619.
[23] M.J. Nine, et al., Graphene: a multipurpose material for protective coatings, J. Mater. Chem. A 3 (24) (2015) 12580–12602.
[24] S.X. Nguyen, et al., Heterojunction of graphene and titanium dioxide nanotube composites for enhancing photocatalytic activity, J. Phys. D. Appl. Phys. 51 (26) (2018), 265304.
[25] V. Singh, et al., Graphene based materials: Past, present and future, Prog. Mater. Sci. 56 (8) (2011) 1178–1271.
[26] D. Losic, D. Tran, S. Kabiri, Composite graphene-based material, 2018 Google Patents.
[27] Z.Q. Wen, et al., Morphology-controlled MnO2–graphene oxide–diatomaceous earth 3-dimensional (3D) composites for high-performance supercapacitors, Dalton Trans. 45 (3) (2016) 936–942.
[28] P. Akshay, et al., Portable and efficient graphene-oxide based multistage filtration unit for water purification, Materials Today: Proceedings 26 (2020) 2344–2350.
[29] X. Wu, et al., Graphene oxide as an efficient antimicrobial nanomaterial for eradicating multi-drug resistant bacteria in vitro and in vivo, Colloids Surf. B: Biointerfaces 157 (2017) 1–9.
[30] M.J. Nine, et al., Interlayer growth of borates for highly adhesive graphene coatings with enhanced abrasion resistance, fire-retardant and antibacterial ability, Carbon 117 (2017) 252–262.
[31] S. Liu, et al., Antibacterial Activity of Graphite, Graphite Oxide, Graphene Oxide, and Reduced Graphene Oxide: Membrane and Oxidative Stress, ACS Nano 5 (9) (2011) 6971–6980.
[32] O. Akhavan, E. Ghaderi, A. Esfandiar, Wrapping Bacteria by Graphene Nanosheets for Isolation from Environment, Reactivation by Sonication, and Inactivation by Near-Infrared Irradiation, J. Phys. Chem. B 115 (19) (2011) 6279–6288.
[33] S. Szunerits, R. Boukherroub, Antibacterial activity of graphene-based materials, J. Mater. Chem. B 4 (43) (2016) 6892–6912.
[34] N. Dubey, et al., Graphene: A Versatile Carbon-Based Material for Bone Tissue Engineering, Stem Cells Int. 2015 (2015) 12.
[35] M. Diba, et al., Electrophoretic deposition of graphene-related materials: A review of the fundamentals, Prog. Mater. Sci. 82 (Supplement C) (2016) 83–117.
[36] Y. Zeng, et al., Graphene oxide/hydroxyapatite composite coatings fabricated by electrochemical deposition, Surf. Coat. Technol. 286 (Supplement C) (2016) 72–79.
[37] H. Ji, H. Sun, X. Qu, Antibacterial applications of graphene-based nanomaterials: Recent achievements and challenges, Adv. Drug Deliv. Rev. 105 (Part B) (2016) 176–189.
[38] Z. Changhong, et al., The promising application of graphene oxide as coating materials in orthopedic implants: preparation, characterization and cell behavior, Biomed. Mater. 10 (1) (2015), 015019.
[39] V.C. Anitha, et al., Enhanced electrochemical performance of morphology-controlled titania-reduced graphene oxide nanostructures fabricated via a combined anodization-hydrothermal process, RSC Adv. 6 (15) (2016) 12571–12583.
[40] W. Liu, et al., Effects of graphene nanosheets on the ceramic coatings formed on Ti6Al4V alloy drill pipe by plasma electrolytic oxidation, J. Alloys Compd. 789 (2019) 996–1007.
[41] S. Singh, et al., Corrosion behaviour of plasma sprayed graphene nanoplatelets reinforced hydroxyapatite composite coatings in simulated body fluid, Ceram. Int. 46 (2020) 13539–13548.
[42] Y. Zuo, et al., Effect of graphene oxide additive on tribocorrosion behavior of MAO coatings prepared on Ti6Al4V alloy, Appl. Surf. Sci. 480 (2019) 26–34.
[43] Y. Gao, et al., Microstructure and Properties of Graphene Oxide-doped TiO2 Coating on Titanium by Micro Arc Oxidation, J. Wuhan Univ. Technol. 33 (6) (2018) 1524–1529.
[44] W. Yang, et al., Preparation of MAO coatings doped with graphene oxide, Surf. Eng. 33 (10) (2017) 739–743.
[45] A. Chavez-Valdez, M.S.P. Shaffer, A.R. Boccaccini, Applications of Graphene Electrophoretic Deposition. A Review, J. Phys. Chem. B 117 (6) (2013) 1502–1515.
[46] L. Besra, M. Liu, A review on fundamentals and applications of electrophoretic deposition (EPD), Prog. Mater. Sci. 52 (1) (2007) 1–61.
[47] X. Chen, et al., Electrochemical behaviour of EPD synthesized graphene coating on titanium alloys for orthopedic implant application, Procedia CIRP 71 (2018) 322–328.
[48] A. Bordbar Khiabani, et al., Electrophoretic deposition of graphene oxide on plasma electrolytic oxidized-magnesium implants for bone tissue engineering applications, Materials Today: Proceedings 5 (7, Part 3) (2018) 15603–15612.
[49] S.A. Ulasevich, et al., Deposition of hydroxyapatite–incorporated TiO2 coating on titanium using plasma electrolytic oxidation coupled with electrophoretic deposition, RSC Adv. 6 (67) (2016) 62540–62544.
[50] X. Nie, A. Leyland, A. Matthews, Deposition of layered bioceramic hydroxyapatite/TiO2 coatings on titanium alloys using a hybrid technique of micro-arc oxidation and electrophoresis, Surf. Coat. Technol. 125 (1) (2000) 407–414.
[51] A. S, et al., The effect of graphite particle size on the corrosion and wear behaviour of the PEO-EPD coating fabricated on commercially pure zirconium, Surf. Coat. Technol. 363 (2019) 301–313.
[52] D.C. Marcano, et al., Improved synthesis of graphene oxide, ACS Nano 4 (8) (2010) 4806–4814.
[53] N.K. Kuromoto, R.A. Simão, G.A. Soares, Titanium oxide films produced on commercially pure titanium by anodic oxidation with different voltages, Mater. Charact. 58 (2) (2007) 114–121.
[54] O.A. Galvis, et al., Formation of grooved and porous coatings on titanium by plasma electrolytic oxidation in H2SO4/H3PO4 electrolytes and effects of coating morphology on adhesive bonding, Surf. Coat. Technol. 269 (2015) 238–249.
[55] S. Aliasghari, P. Skeldon, G.E. Thompson, Plasma electrolytic oxidation of titanium in a phosphate/silicate electrolyte and tribological performance of the coatings, Appl. Surf. Sci. 316 (2014) 463–476.
[56] I. Ali, et al., One-step electrochemical synthesis of graphene oxide-TiO2 nanotubes for improved visible light activity, Opt. Mater. Express 7 (5) (2017) 1535–1546.
[57] T. Kokubo, H. Takadama, How useful is SBF in predicting in vivo bone bioactivity? Biomaterials 27 (15) (2006) 2907–2915.
[58] P. Richiez-Nieves, et al., A Sheep Model for the Osseointegration of PEO-treated Gamma Titanium Aluminide, Eur. J. Dental Oral Health 1 (2020).
[59] M. Echeverry-Rendón, et al., Osseointegration improvement by plasma electrolytic oxidation of modified titanium alloys surfaces, J. Mater. Sci. Mater. Med. 26 (2) (2015) 72.
[60] M. Diba, et al., Electrophoretic deposition of graphene-related materials: A review of the fundamentals, Prog. Mater. Sci. 82 (2016) 83–117.
[61] V. Malinovschi, et al., Obtaining and characterization of PEO layers prepared on CP-Ti in sodium dihydrogen phosphate dihydrate acidic electrolyte solution, Surf. Coat. Technol. 375 (2019) 621–636.
[62] S. Shalini, et al., Effect of Na doping on structure, morphology and properties of hydrothermally grown one dimensional TiO2 nanorod structures, J. Mater. Sci. Mater. Electron. 28 (4) (2017) 3500–3508.
[63] Hussein, R.O., et al., 2010: p. 105203-105216.
[64] M. Uchida, et al., Structural dependence of apatite formation on titania gels in a simulated body fluid, J. Biomed. Mater. Res. Part A 64 (1) (2003) 164–170.
[65] J. Qiu, et al., Combination types between graphene oxide and substrate affect the antibacterial activity, Bioactive Materials 3 (3) (2018) 341–346.
[66] Q. Zhou, et al., Bioactivity of periodontal ligament stem cells on sodium titanate coated with graphene oxide, Sci. Rep. 6 (2016) 19343.
[67] U. Kiran, et al., Graphene Coating on Copper by Electrophoretic Deposition for Corrosion Prevention, Coatings 7 (2017).
[68] A. Janković, et al., Graphene-based antibacterial composite coatings electrodeposited on titanium for biomedical applications, Prog. Org. Coat. 83 (2015) 1–10.
[69] A.L. Hook, et al., Combinatorial discovery of polymers resistant to bacterial attachment, Nat. Biotechnol. 30 (9) (2012) 868–875.
[70] T. Merian, J.M. Goddard, Advances in nonfouling materials: perspectives for the food industry, J. Agric. Food Chem. 60 (12) (2012) 2943–2957.

[71] L. Fang, et al., Effects of oxidation time on microstructure and corrosion resistance of micro-arc oxidation film on aluminum alloy, Fenmo Yejin Cailiao Kexue yu Gongcheng/Materials Science and Engineering of Powder Metallurgy 23 (5) (2018) 503–510.
[72] Y. Jiang, Y. Bao, K. Yang, Composite Coatings Combining PEO Layer and EPD Layer on Magnesium Alloy, Magnesium Technology, Springer 2011, pp. 543–546.
[73] X. Ma, et al., A model describing the growth of a PEO coating on AM50 Mg alloy under constant voltage mode, Electrochim. Acta 251 (2017) 461–474.
[74] E. Matykina, et al., In vitro corrosion performance of PEO coated Ti and Ti6Al4V used for dental and orthopaedic implants, Surf. Coat. Technol. 307 (2016) 1255–1264.
[75] M. haghbin nazarpak, et al., Effect of Gamma Irradiation on Structural and Biological Properties of a PLGA-PEG-Hydroxyapatite Composite, Sci. World J. 2014 (2014).
[76] S. Raynaud, et al., Calcium phosphate apatites with variable Ca/P atomic ratio I. Synthesis, characterisation and thermal stability of powders, Biomaterials 23 (4) (2002) 1065–1072.
[77] X. Liu, C. Ding, Z. Wang, Apatite formed on the surface of plasma-sprayed wollastonite coating immersed in simulated body fluid, Biomaterials 22 (14) (2001) 2007–2012.
[78] M. Mehrali, et al., Electrophoretic deposition of calcium silicate–reduced graphene oxide composites on titanium substrate, J. Eur. Ceram. Soc. 36 (2) (2016) 319–332.
[79] V.A. Ponomarev, et al., Ag(Pt) nanoparticles-decorated bioactive yet antibacterial Ca- and P-doped TiO2 coatings produced by plasma electrolytic oxidation and ion implantation, Appl. Surf. Sci. 516 (2020), 146068.
[80] O. Akhavan, E. Ghaderi, Toxicity of Graphene and Graphene Oxide Nanowalls Against Bacteria, ACS Nano 4 (10) (2010) 5731–5736.
[81] R. Silva-Leyton, et al., Polyethylene/graphene oxide composites toward multifunctional active packaging films, Compos. Sci. Technol. 184 (2019), 107888.
[82] H. Ji, H. Sun, X. Qu, Antibacterial applications of graphene-based nanomaterials: Recent achievements and challenges, Adv. Drug Deliv. Rev. 105 (2016) 176–189.
[83] F. Perreault, et al., Antimicrobial Properties of Graphene Oxide Nanosheets: Why Size Matters, ACS Nano 9 (7) (2015) 7226–7236.
[84] N. Yadav, et al., Graphene Oxide-Coated Surface: Inhibition of Bacterial Biofilm Formation due to Specific Surface–Interface Interactions, ACS Omega 2 (7) (2017) 3070–3082.